Cancer Letters 457 (2019) 151–167

Contents lists available at ScienceDirect

Cancer Letters

journal homepage: www.elsevier.com/locate/canlet

Original Articles

A feedforward relationship between active Rac1 and phosphorylated Bcl-2 is critical for sustaining Bcl-2 phosphorylation and promoting cancer progression

Stephen Jun Fei Chong[a,b], Jolin Xiao Hui Lai[a], Jianhua Qu[a,b], Jayshree Hirpara[d], Jia Kang[a,c], Kunchithapadam Swaminathan[e], Thomas Loh[f], Ansu Kumar[g], Shireen Vali[h], Taher Abbasi[h], Shazib Pervaiz[a,b,c,i,*]

[a] Department of Physiology, Yong Loo Lin School of Medicine, National University of Singapore (NUS), Singapore
[b] Medical Science Cluster Cancer Program, Yong Loo Lin School of Medicine, National University of Singapore (NUS), Singapore
[c] NUS Graduate School of Integrative Sciences and Engineering, NUS, Singapore
[d] Cancer Science Institute, NUS, Singapore
[e] Department of Biological Sciences, National University of Singapore (NUS), Singapore
[f] Department of Otolaryngology, National University Healthcare System (NUHS), Singapore
[g] Cellworks Research India Private Limited, Bangalore, India
[h] Cellworks Group Inc., San Jose, CA, USA
[i] National University Cancer Institute, NUHS, Singapore

ARTICLE INFO

Keywords:
Active Rac1
Bcl-2 phosphorylation
Reactive oxygen species
Cancer
Chemo-resistance

ABSTRACT

Active GTPase-Rac1 is associated with cellular processes involved in carcinogenesis and expression of Bcl-2 endows cells with the ability to evade apoptosis. Here we provide evidence that active Rac1 and Bcl-2 work in a positive feedforward loop to promote sustained phosphorylation of Bcl-2 at serine-70 (S70pBcl-2), which stabilizes its anti-apoptotic activity. Pharmacological and genetic inactivation of Rac1 prevent interaction with Bcl-2 and reduce S70pBcl-2. Similarly, BH3-mimetic inhibitors of Bcl-2 could disrupt Rac1-Bcl-2 interaction and reduce S70pBcl-2. This effect of active Rac1 could also be rescued by scavengers of intracellular superoxide ($O_2^{\cdot -}$), thus implicating NOX-activating activity of Rac1 in promoting S70pBcl-2. Moreover, active Rac1-mediated redox-dependent S70pBcl-2 involves the inhibition of phosphatase PP2A holoenzyme assembly. Sustained S70pBcl-2 in turn secures Rac1/Bcl-2 interaction. Importantly, inhibiting Rac1 activity, scavenging $O_2^{\cdot -}$ or employing BH3-mimetic inhibitor significantly reduced S70pBcl-2-mediated survival in cancer cells. Notably, Rac1 expression, and its interaction with Bcl-2, positively correlate with S70pBcl-2 levels in patient-derived lymphoma tissues and with advanced stage lymphoma and melanoma. Together, we provide evidence of a positive feedforward loop involving active Rac1, S70pBcl-2 and PP2A, which could have potential diagnostic, prognostic and therapeutic implications.

1. Introduction

Apoptosis resistance is a hallmark of cancer, which is partly dictated by an altered redox metabolism [1–3]. In particular, a pro-oxidant intracellular milieu endows cells the ability to evade death signals and promote pro-survival networks [2,4–7]. In this case, our previous work has highlighted that a slight increase in intracellular superoxide ($O_2^{\cdot -}$) could protect cancer cells from death-inducing stimuli such as staurosporine and etoposide [5,8,9]. To that end, we previously linked the activation of Rac1 (GTP-loaded) [10] to inhibition of apoptosis via its ability to trigger NADPH oxidase (NOX)-mediated $O_2^{\cdot -}$ production [8]. Supporting its oncogenic role, Rac1 overexpression has also been reported in various malignancies including lymphoma, leukemia and breast cancer [11–13]. Intriguingly, the death-inhibitory activity of the anti-apoptotic B-cell lymphoma/leukemia-2 (Bcl-2) protein is also linked to its ability to induce a pro-oxidant intracellular milieu through an increase in mitochondrial $O_2^{\cdot -}$ [9,14–16]. Notably, inhibiting Rac1 activity or its gene knockdown not only alleviates $O_2^{\cdot -}$ production but

* Corresponding author. Department of Physiology, Yong Loo Lin School of Medicine, National University of Singapore, 2 Medical Drive, MD9 #01-05, 117597, Singapore.
E-mail address: phssp@nus.edu.sg (S. Pervaiz).

https://doi.org/10.1016/j.canlet.2019.05.009
Received 8 January 2019; Received in revised form 15 April 2019; Accepted 8 May 2019
0304-3835/ © 2019 Elsevier B.V. All rights reserved.

Abbreviation list

S70pBcl-2	Serine-70 phosphorylated Bcl-2
$O_2^{\cdot-}$	Superoxide anion
Bcl-2	B-cell lymphoma/leukemia-2
PP2A	Protein Phosphatase-2A
PLA	Proximity Ligation Assay
$ONOO^-$	Peroxynitrite
DPI	Diphenyleneiodonium
NOX	NADPH Oxidase
ROS	Reactive Oxygen Species
ABT199	Venetoclax

also restores apoptotic signaling in Bcl-2 overexpressing cancer cells [8]. This regulatory effect of Rac1 on Bcl-2-mediated $O_2^{\cdot-}$ production was later shown to involve interaction between the two pro-oncogenic proteins in cell lines and primary cells from lymphoma patients [9].

The Bcl-2 protein possesses a putative unstructured loop, adjacent to its BH3 domain, that is important for its anti-apoptotic function [17]. This region contains the serine-70 residue that is amenable to phosphorylation [5,17–24]. To that end, our recent work showed that Bcl-2 phosphorylation at serine-70 (S70pBcl-2) promoted apoptosis resistance in cancer cells [5]. More relevantly, we showed that S70pBcl-2 was mediated by peroxynitrite ($ONOO^-$)-generated by the reaction of $O_2^{\cdot-}$ with nitric oxide (NO)-which nitrates the Bcl-2-recognizing and -bound B56δ subunit of protein phosphatase-2A (PP2A) and prevents its assembly with the catalytic core of PP2A. This in turn inactivates the PP2A activity and permits the accumulation of S70pBcl-2, thereby sustaining the anti-apoptotic activity of Bcl-2 [5]. Intriguingly, Rac1 has also been implicated in S70pBcl-2 induction via JNK activation [25].

Despite these findings, the activation status and redox activity of Rac1 in the interaction with Bcl-2 and induction of S70pBcl-2 remain elusive. Similarly, although $O_2^{\cdot-}$-induced inhibition of PP2A assembly promotes chemo-resistance via sustained S70pBcl-2, the relationship between Rac1 and PP2A in the context of pro-oxidant state, S70pBcl-2 and Rac1/Bcl-2 interaction is unknown. Also, the involvement of phosphorylation sensitive serine-70 residue in the interaction with Rac1 has yet to be elucidated.

Here we provide evidence that active Rac1 (GTP-bound) binds to Bcl-2, which subsequently permits the accumulation of S70pBcl-2 via redox-mediated inhibition of PP2A assembly. Increased S70pBcl-2 levels in turn secure the interaction between Rac1 and Bcl-2, thereby suggesting a feedforward loop that could sustain S70pBcl-2 and elicit apoptosis resistance. Importantly, data from patient-derived primary lymphoma cells strongly support our *in vitro* work as well as provide significant evidence of association with advanced disease stage in lymphoma and melanoma patients.

2. Materials and methods

Detailed materials and methods can be found in supplementary text.

2.1. Cell lines

Human leukemia CEM cells stably expressing pcDNA3.1 vector containing either the neomycin (CEM/Neo) or human Bcl-2 and neomycin genes (CEM/Bcl-2) were cultured in RPMI-1640 (10%FBS, 2 mM L-Glut, 20 μg/ml antibiotic G418). Human leukemia Jurkat cells were cultured in RPMI-1640 (10%FBS, 2 mM L-Glut). Human M14 melanoma cells stably expressing pIRES vector containing either the hygromycin or constitutively active human Rac1 mutant and hygromycin gene (G12V), were cultured in DMEM (10%FBS, 2 mM L-Glut, 0.5%antibiotic hygromycin-B). Cell lines were authenticated by Short Tandem Repeat method, from Transcend (NUHS) and Promega.

2.2. Proximity ligation assay

The Duolink® In-Situ Red Starter Kit Mouse/Rabbit was purchased from Sigma Aldrich (Cat.#DUO92101). Aside from the 24-h primary antibody incubation, the assay was performed according to manufacturer's protocol. Prepared samples were subsequently imaged for red signals with confocal microscopy for indication of protein-protein interaction.

2.3. 3D-spheroid formation assay

2000 cells in fresh 200 μl antibiotic-free medium (2 mM L-glutamine and 10%FBS) was seeded on a 96-format spheroid microplate (triplicate/sample)(Corning®) following drug treatments and incubated for 72 h at 37 °C, 5%CO_2, 95%humidity. Images of spheroid sizes were then captured under light microscope (Carl Zeiss). Areas of spheroids were calculated using Carl Zeiss ZEN-2 (Blue version) software.

2.4. Rac1 activation assay

1million cells were harvested following seeding or treatment of NSC23766 for colorimetric-based Rac1 activity assay. Assay was performed according to manufacturer's protocol (Cytoskeleton, Cat.#BK128).

3. Results

3.1. Active Rac1-induced Rac1/Bcl-2 interaction is implicated in S70pBcl-2 induction

A previous report suggested the involvement of active Rac1 in the phosphorylation of Bcl-2 albeit in monkey kidney fibroblast-like cells (COS-7) [25], however, the underlying mechanism(s) particularly from the standpoint of redox-modifying activity of Rac1 remains obscure. Similarly, although Rac1 has been shown to interact with Bcl-2 [9],

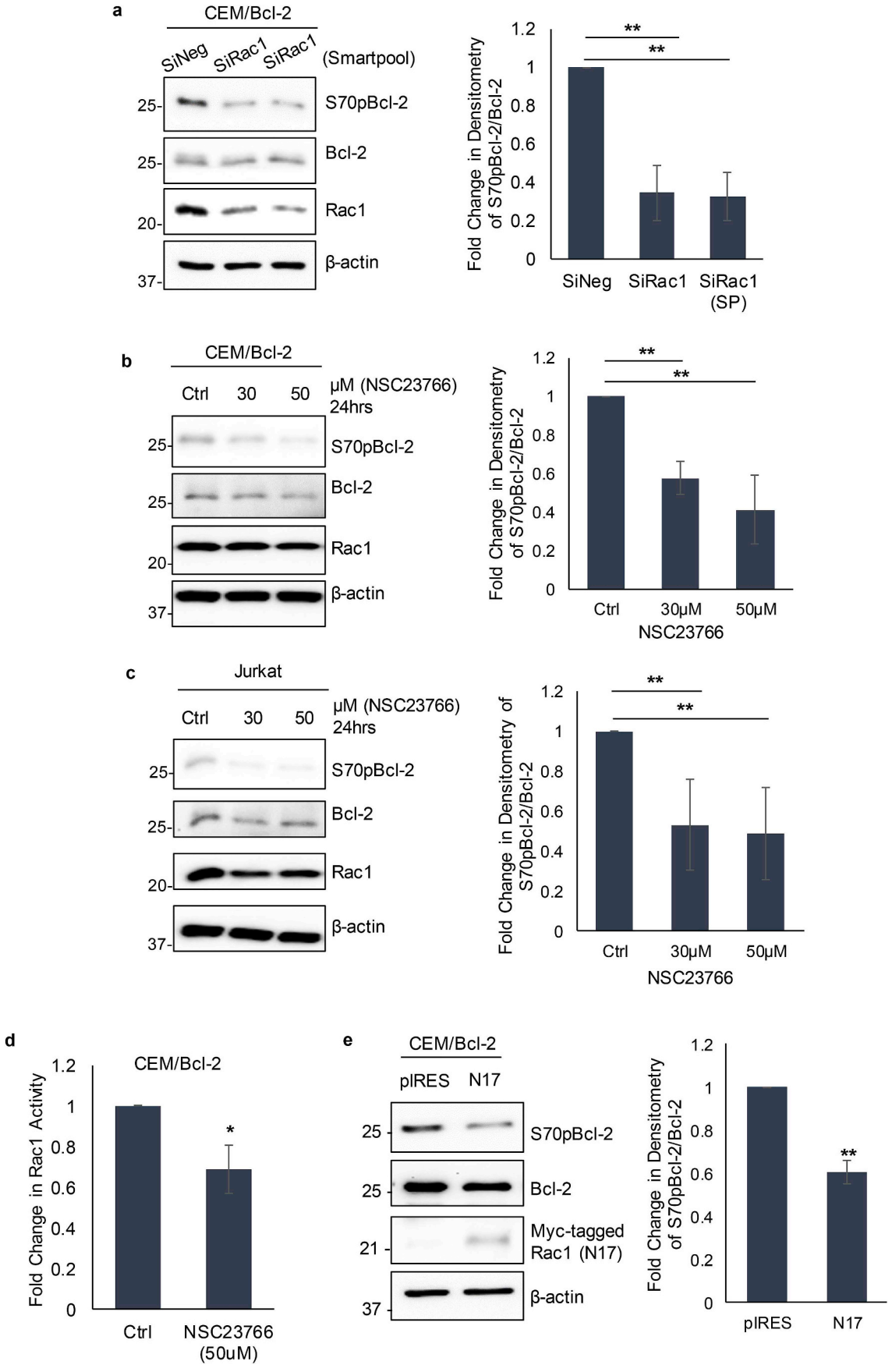

(caption on next page)

Fig. 1. Rac1 is implicated in S70 phosphorylation of Bcl-2.
(a) Western Blot analysis showing S70pBcl-2, Bcl-2, Rac1 and β-actin following 48-h Rac1 knockdown with either a Rac1 specific siRNA sequence or a Rac1 specific siRNA smartpool (150 nM) in CEM leukemia cells stably overexpressing Bcl-2 (CEM/Bcl-2). n = 4. Bar chart showing fold change in densitometry of S70pBcl-2 normalized to Bcl-2. (b–c) Western Blot analysis showing S70pBcl-2, Bcl-2, Rac1 and β-actin following 24-h treatment of increasing dose of Rac1 inhibitor, NSC23766, in CEM/Bcl-2 and Jurkat cells. n = 3, n = 5 respectively. Bar charts showing fold change in densitometry of S70pBcl-2 normalized to Bcl-2. (d) Measurement of Rac1 activity following 24-h treatment of 50 μM NSC23766 in CEM/Bcl-2 cells. n = 3. (e) Western Blot analysis showing S70pBcl-2, Bcl-2, Myc-tagged Rac1 (N17) and β-actin in CEM/Bcl-2 cells transiently transfected with Myc-tagged dominant negative Rac1 mutant, N17, or empty vector, pIRES. n = 3. Bar chart showing fold change in densitometry of S70pBcl-2 normalized to Bcl-2. All bar charts displaying mean and SD. Paired T-test was used for experiments with 2 samples. One way-ANOVA and Tukey's multiple comparisons tests were used for experiments with more than 2 samples. * and ** indicate P-value < 0.05 and < 0.02 respectively.

there is no evidence to demonstrate if an active GTP-bound Rac1 is crucial for its interaction with Bcl-2 as well as a prerequisite for the induction of S70pBcl-2. Intrigued by these mechanistic gaps, we proceeded to investigate the possibility of a physical crosstalk between active Rac1 and Bcl-2 in S70pBcl-2 induction. Firstly, we confirmed the involvement of active Rac1 in promoting S70pBcl-2 in CEM and Jurkat leukemia as well as M14 melanoma cancer cells. We genetically knocked down *RAC1* with a single sequence-specific or smart-pool siRNA in Bcl-2 overexpressing CEM cells (CEM/Bcl-2), or inhibited Rac1 activation with NSC23766 or transiently expressed the dominant negative mutant $Rac1^{T17N}$ ($Rac1^{N17}$) in CEM/Bcl-2 and Jurkat cells. Conversely, constitutively active $Rac1^{G12V}$ ($Rac1^{V12}$) was stably expressed in M14 melanoma cells. Indeed, we observed that gene knock down of *RAC1* or $Rac1^{N17}$ expression as well as pharmacological inhibition of Rac1 activity reduced S70pBcl-2 in CEM/Bcl-2 and Jurkat cells (Fig. 1a–c, 1e). Rac1 inhibition with NSC23766 was also accompanied by reduced Rac1 activity (Fig. 1d, S1; positive control). On the other hand, stable overexpression of $Rac1^{V12}$ showed enhanced S70pBcl-2 in M14 cells (Fig. S2). These data collectively implicate active Rac1 in sustaining S70pBcl-2 in cancer cells.

Given that Rac1-induced S70pBcl-2 is implicated in cancer cells, we proceeded to investigate if active Rac1 is required for the physical interaction between Rac1 and Bcl-2. Indeed, co-IP analysis showed that inhibition of Rac1 activation by NSC23766 or transient transfection of $Rac1^{N17}$ prevented the interaction between Rac1 and Bcl-2 in CEM/Bcl-2 cells. This is accompanied by a reduction in S70pBcl-2 (Fig. 2a, S3a). As S70pBcl-2 stabilizes the anti-apoptotic activity of Bcl-2, we observed that S70pBcl-2 reduction also resulted in a decrease in Bcl-2 sequestration of the BH3-only pro-apoptotic protein NOXA (Figs. S3a–b). Reciprocally, co-IP analysis and PLA revealed interaction between Rac1 and Bcl-2 (Fig. 2b–d) as well as higher S70pBcl-2 (Fig. 2b) in constitutively active $Rac1^{V12}$ M14 cells, compared to pIRES vector-transfected cells. Similarly, sustained S70pBcl-2 facilitates binding to NOXA (Fig. S3c). In addition, blank samples of PLA with only secondary antibodies or IgG controls for co-IP showed absence of non-specific signals (Fig. 2c–d, S3d). To ascertain that active Rac1-induced interaction is important for sustained S70pBcl-2, we proceeded to use two different Bcl-2 inhibitors, HA14-1 and BH3-mimetic ABT199 (venetoclax), to disrupt the interaction between Rac1 and Bcl-2 (Fig. 2e–f). Indeed, as Rac1/Bcl-2 interaction is reduced by either HA14-1 or ABT199, we observed a significant decrease in S70pBcl-2 in CEM/Bcl-2 cells (Fig. 2g–h). This is similarly seen in Jurkat cells treated with ABT199 (Fig. S4). Together, these results show that active Rac1-mediated interaction with Bcl-2 is implicated in sustained S70pBcl-2.

3.2. Rac1-induced S70pBcl-2 is ROS-dependent

Active Rac1 is involved in NOX-dependent intracellular $O_2^{\cdot-}$ production [8]. Therefore, we asked if scavenging $O_2^{\cdot-}$ would similarly reduce S70pBcl-2. Indeed, treatment with $O_2^{\cdot-}$ scavenger, tiron (5–10 mM, 24 h), inhibited S70pBcl-2 in CEM/Bcl-2 and Jurkat cells (Fig. 3a–b). Similarly, treatment with NOX inhibitor, diphenyleneiodonium (DPI), reduced S70pBcl-2 in Jurkat cells (Fig. 3c). Reciprocally, M14 $Rac1^{V12}$ cells that displayed higher intracellular $O_2^{\cdot-}$ levels concurrently showed a higher S70pBcl-2 level (Fig. 3d and f). Treatment with tiron (10 mM, 24 h) not only reversed the increased intracellular $O_2^{\cdot-}$ but also reduced S70pBcl-2 levels in M14 $Rac1^{V12}$ cells (Fig. 3e–f). Importantly, the reduction of Bcl-2 phosphorylation is specific to S70pBcl-2 as residue such as T69pBcl-2 was not affected (Fig. S5). These data link active Rac1 and its downstream $O_2^{\cdot-}$ production to sustained S70pBcl-2.

3.3. Active Rac1 sustains S70pBcl-2 via redox-dependent inhibition of PP2A assembly

Given that Rac1-induced ROS is critical for S70pBcl-2 induction, we next examined if Rac1-induced S70pBcl-2 via $O_2^{\cdot-}$ is JNK-dependent. As shown in Fig. 4a, tiron failed to inhibit JNK activation as shown by its unchanged phosphor-activating status, indicating that Rac1-induced S70pBcl-2 via $O_2^{\cdot-}$ is independent of JNK. Interestingly, we recently uncovered a novel mechanism underlying $O_2^{\cdot-}$-dependent S70pBcl-2 that involved $ONOO^-$-induced nitration of the Bcl-2-regulatory B56δ subunit. This inhibited the assembly of B56δ to the catalytic core of PP2A, thereby inactivating PP2A and preventing the dephosphorylation of S70pBcl-2 [5]. Stimulated by our findings linking active Rac1-induced $O_2^{\cdot-}$ to sustained S70pBcl-2, we asked whether a similar PP2A-dependent mechanism was operative in mediating the effect of active Rac1. To do so, M14 $Rac1^{V12}$ cells were incubated with increasing

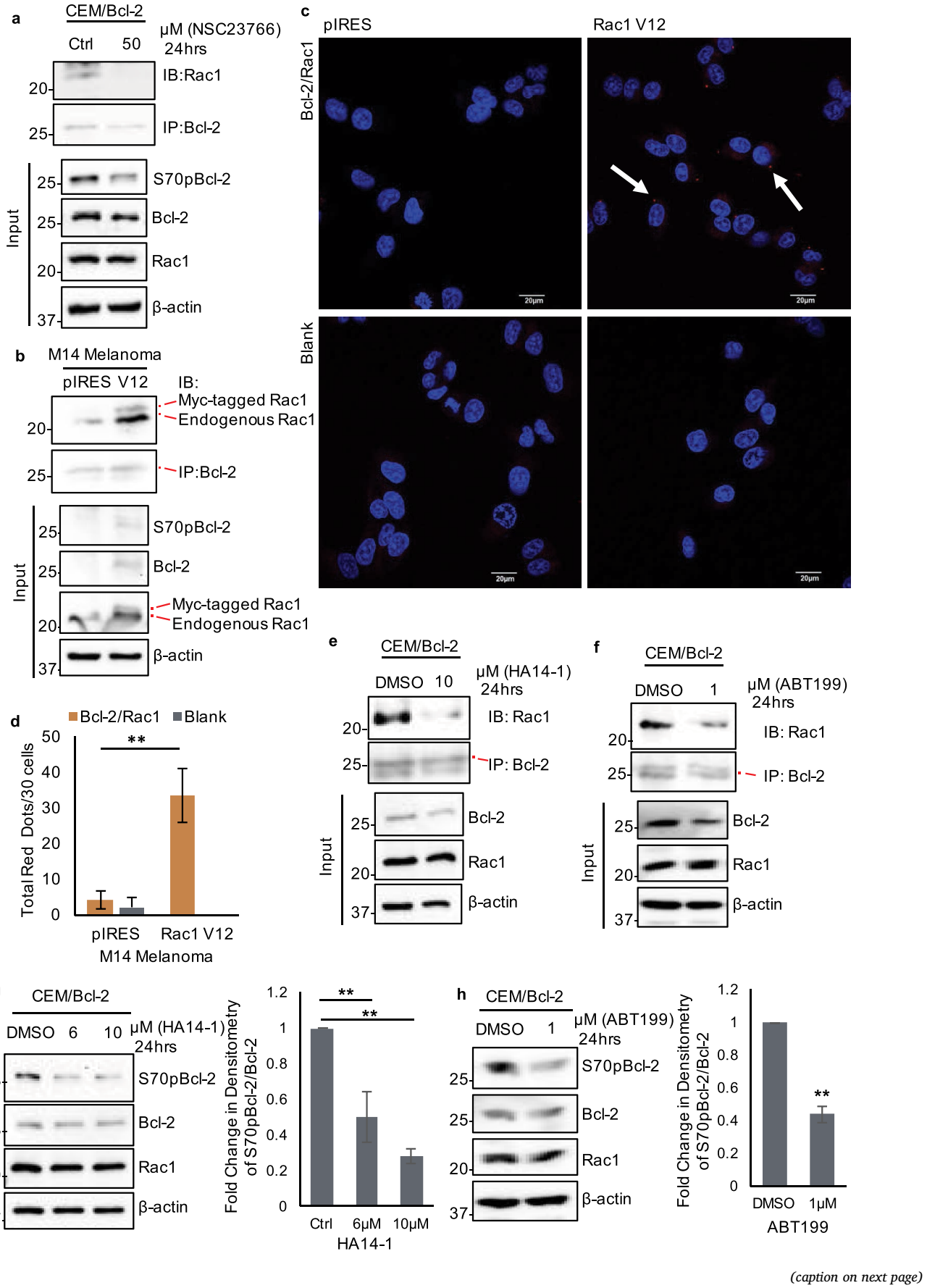

(caption on next page)

Fig. 2. Active Rac1 is implicated in Rac1/Bcl-2 interaction for the induction of S70 phosphorylation of Bcl-2.
(a) Western blot analysis showing the immunoprecipitation of Bcl-2 and immunoblotting of Rac1 and their respective immunoblotted inputs of S70pBcl-2, Bcl-2, Rac1 and β-actin following 24-h treatment of 50 μM NSC23766 in CEM/Bcl-2 cells. n = 3. Rac1 was first immunoblotted followed by Bcl-2. This immunoblotting sequence is similar in all Rac1/Bcl-2 co-immunoprecipitation analyses. (b) Western blot analysis showing the immunoprecipitation of Bcl-2 and immunoblotting of Rac1 and their respective immunoblotted inputs of S70pBcl-2, Bcl-2, Rac1 and β-actin in M14 Melanoma cells stably expressing the Myc-tagged constitutively active Rac1 mutant, V12, or empty vector, pIRES. n = 3. (c) Proximity ligation assay (PLA) showing red dot appearances (white arrow) upon Bcl-2 and Rac1 interaction of pIRES and Rac1 V12 M14 Melanoma cells. Red dots were calculated from 30 cells from randomly selected images. Blank images indicate only secondary antibodies used to check for non-specific signal. n = 3. (d) Quantification of total red dots from 30 cells from randomly selected images for target and blank samples of 3 independent sets. (e–f) Western blot analysis showing the immunoprecipitation of Bcl-2 and immunoblotting of Rac1 and their respective immunoblotted inputs of Bcl-2, Rac1 and β-actin following 24-h treatment of 10 μM HA14-1 or 1 μM ABT199 in CEM/Bcl-2 cells. n = 3. (g) Western Blot analysis showing S70pBcl-2, Bcl-2, Rac1 and β-actin following 24-h treatment of increasing doses of BH3 mimetic, HA14-1, in CEM/Bcl-2 cells. n = 4. Bar chart showing fold change in densitometry of S70pBcl-2 normalized to Bcl-2. (h) Western Blot analysis showing S70pBcl-2, Bcl-2, Rac1 and β-actin following 24-h treatment of 1 μM Bcl-2-specific BH3 mimetic, ABT-199, in CEM/Bcl-2 cells. n = 4. Bar chart showing fold change in densitometry of S70pBcl-2 normalized to Bcl-2. All bar charts displaying mean and SD. Paired T-test was used for experiments with 2 samples. One way-ANOVA and Tukey's multiple comparisons tests were used for experiments with more than 2 samples. ** indicates P-value < 0.02. (For interpretation of the references to color in this figure legend, the reader is referred to the Web version of this article.)

concentrations of FeTPPS, a $ONOO^-$ decomposition catalyst. Indeed, a dose-dependent decrease in S70pBcl-2 was observed (Fig. 4b), thereby prompting us to explore the involvement of PP2A. To that end, results show that B56δ subunit recruitment to the catalytic subunit (C-subunit) of PP2A was inhibited in M14 $Rac1^{V12}$ cells (Fig. 4c). IgG control is displayed in Supplementary Fig. S6. Furthermore, we provide evidence that, similar to our recent findings in hematopoietic cells [5], B56δ is also the regulatory subunit that binds to S70pBcl-2 (for its subsequent dephosphorylation) in M14 cells (Fig. 4d). Supporting that, a significant increase in S70pBcl-2 is detected in cells upon B56δ knockdown (Fig. 4d; Input). To further corroborate our co-IP data on B56δ/C-subunit interaction, PLA with B56δ and C-subunit proteins in M14 pIRES cells showed significantly more interacting signals (red) as compared to that of $Rac1^{V12}$ (Fig. 4e–f). Importantly, treatment of ABT199, shown to prevent the binding of Bcl-2 to Rac1 (Fig. 2f), enhanced the binding of B56δ to its C-subunit, while concurrently interacting with Bcl-2 in CEM/Bcl-2 cells (Fig. 4g). Similarly, tiron could prevent the inhibition of B56δ recruitment to the C-subunit, while in the presence of Bcl-2, in M14 $Rac1^{V12}$ cells (Fig. 4h). Collectively, these data implicate Rac1/Bcl-2 interaction in the redox-mediated inhibition of PP2A assembly and S70pBcl-2 dephosphorylation.

3.4. S70pBcl-2 secures the interaction between Rac1 and Bcl-2

Intriguingly, scavenging Rac1-induced $O_2^{\cdot-}$ not only reduced S70pBcl-2 but also decreased Rac1/Bcl-2 interaction (Fig. 5a), thereby suggesting that S70pBcl-2 could have an additional role in stabilizing the interaction between the two proteins. To verify this, we transiently overexpressed wild-type (WT) Bcl-2 in M14 cells and artificially clamped down S70pBcl-2 via pharmacological inhibition of JNK (SP600125); JNK phosphorylates Bcl-2 independent of $O_2^{\cdot-}$. A dose-dependent decrease in S70pBcl-2 and downstream target of JNK, phospho-c-Jun, were observed following 6hour-treatment of SP600125 (Fig. 5b, S7a). Similar effects of JNK inhibition were observed in M14 $Rac1^{V12}$ cells (Fig. S7b). Importantly, the decrease in S70pBcl-2 also correlates with the decrease in Rac1/Bcl-2 interaction (Fig. 5c), thereby suggesting that S70pBcl-2 could further stabilize this protein-protein interaction.

To ascertain this hypothesis, we performed co-IP-Western analyses upon transient overexpression of WT Bcl-2, phosphorylation-inefficient mutant (S70A) or phosphomimetic mutant (S70E) in M14 cells. Our data show a significant increase in S70pBcl-2 in S70E-transfected cells, and most noticeably strong Rac1/Bcl-2 interaction (Fig. 5d), which was absent in S70A-transfected cells (Fig. 5e). It is also worth mentioning that the increase in Rac1/Bcl-2 interaction in WT Bcl-2-transfected cells could be attributed to the increased endogenous S70pBcl-2 (Fig. 5d–e; inputs). Notably, as S70E mutant displayed an enhanced S70pBcl-2 compared to WT Bcl-2, this suggests that the S70 phospho-specific antibody could cross-react with S70E phosphomimetic mutant. This is supported by the authenticity of the antibody as Bcl-2 knockdown could eliminate S70pBcl-2 in Jurkat cells expressing WT Bcl-2 or S70E as well as sequencing of S70E plasmid verified the site-directed mutation (Figs. S8a–b).

Corroborating our co-IP data, PLA with Bcl-2 and Rac1 proteins in CEM cells transiently overexpressing the S70E and WT Bcl-2 showed significantly more interacting signals (red) as compared to that of S70A and pcDNA3.1 (Fig. 5f–g, S8c; successful transfection). Collectively, these findings indicate an additional role of S70pBcl-2 in securing the interaction between Rac1 and Bcl-2, thereby suggesting a positive feedforward loop that involves the interaction between active Rac1 and Bcl-2 to permit redox-mediated inactivation of PP2A and subsequent accumulation of S70pBcl-2, which in turn further secures the

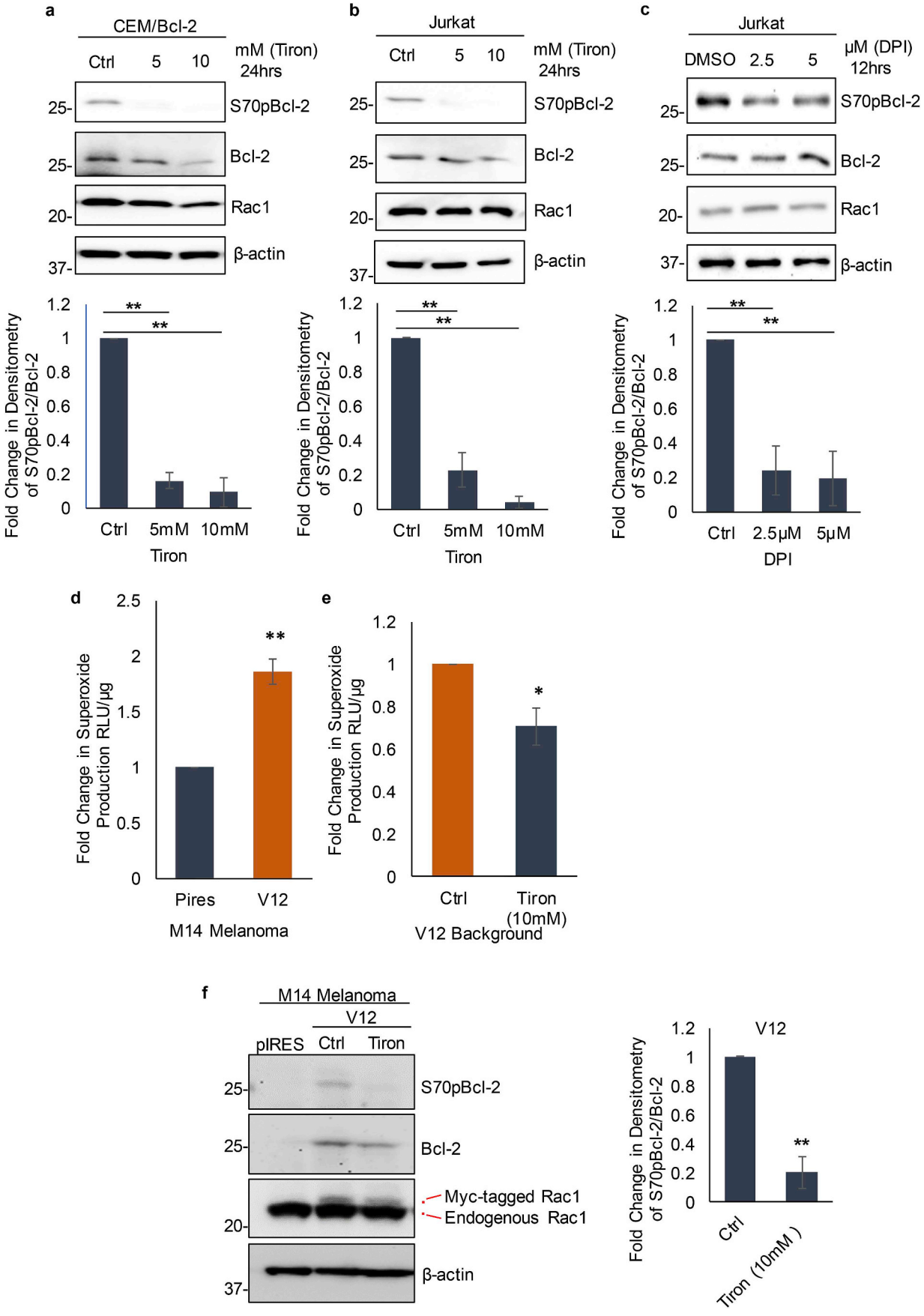

(caption on next page)

Fig. 3. Rac1-induced S70 phosphorylation of Bcl-2 is ROS-dependent.
(a–b) Western Blot analysis showing S70pBcl-2, Bcl-2, Rac1 and β-actin following 24-h treatment of increasing doses of Tiron in CEM/Bcl-2 and Jurkat cells. n = 4. Bar charts showing fold change in densitometry of S70pBcl-2 normalized to Bcl-2. (c) Western Blot analysis showing S70pBcl-2, Bcl-2, Rac1 and β-actin following 12-h treatment of increasing doses of DPI in Jurkat cells. n = 4. Bar chart showing fold change in densitometry of S70pBcl-2 normalized to Bcl-2. (d) Measurement of $O_2^{\cdot-}$ production in M14 Melanoma cells stably expressing the Myc-tagged constitutively active Rac1 mutant, V12, or empty vector, pIRES. n = 3. (e) Measurement of $O_2^{\cdot-}$ production following 24-h treatment of 10 mM Tiron in M14 Melanoma cells stably expressing the Myc-tagged constitutively active Rac1 mutant, V12. n = 3. (f) Western Blot analysis showing S70pBcl-2, Bcl-2, Rac1 and β-actin following 24-h treatment of 10 mM Tiron in M14 Melanoma cells stably expressing the Myc-tagged constitutively active Rac1 mutant, V12. pIRES served as control. n = 4. Bar chart showing fold change in densitometry of S70pBcl-2 normalized to Bcl-2. All bar charts displaying mean and SD. Paired T-test was used for experiments with 2 samples. One way-ANOVA and Tukey's multiple comparisons tests were used for experiments with more than 2 samples. * and ** indicate P-value < 0.05 and < 0.02 respectively.

interaction between Rac1 and Bcl-2.

3.5. Pharmacological disruptions of the Active Rac1-S70pBcl-2 feedforward loop sensitizes cancer cell to apoptosis

To understand the functional relevance of our findings in the context of cancer cell fate, we next investigated the effect of disrupting this feedforward loop on cancer cell response to apoptotic stimuli. Indeed, *in silico RAC1* knockdown, a computational simulation generated by Cellworks™, or *in vitro* Rac1 inhibition (NSC23766, 24 h) resulted in a significant reduction in viability of CEM/Bcl-2 and Jurkat cells (Fig. 6a–b, S9a-b, S10). Alternatively, $Rac1^{V12}$ expression endowed M14 cells the ability to resist staurosporine-induced apoptosis (Fig. 6c). As $Rac1^{V12}$ upregulates S70pBcl-2 via an increase in intracellular $O_2^{\cdot-}$, we then evaluated the effect of scavenging $O_2^{\cdot-}$ on drug sensitivity. Indeed, *a priori* treatment of $Rac1^{V12}$ cells with tiron for 1 h significantly increased the sensitivity of cells to staurosporine (24 h) (Fig. 6c). As we showed that ABT199 could similarly reduce S70pBcl-2, a similar pre-treatment with non-cytotoxic concentration of ABT199 (1 μM) for 1 h synergized with non-cytotoxic concentration of staurosporine (50 nM, 24 h) in decreasing the viability of CEM/Bcl-2 cells (Fig. 6d). Reciprocally, transient overexpression of S70E and to a lesser extent WT Bcl-2, but not S70A, protected M14 cells from staurosporine-induced cell death (Fig. 6e). These data were further corroborated by assaying the ability of 2000 cells to survive, proliferate and form 3D-spheroids in 72 h following similar treatments. 3D-spheroid formed by $Rac1^{V12}$-expressing M14 cells was minimally affected by staurosporine. However, pre-treatment with tiron resulted in a significant reduction in spheroid-forming ability, thereby providing testimony to the involvement of intracellular $O_2^{\cdot-}$ in apoptosis resistance induced by active Rac1 (Fig. 6f–g). More importantly, the effect of staurosporine on 3D-spheroid formation was significantly blocked by transient expression of S70E, whereas S70A mutant had no significant effect in M14 cells (Fig. 6h–i). We also verified the status of S70pBcl-2 under all treatment conditions. Notably, scavenging $O_2^{\cdot-}$ (tiron) or preventing Rac1/Bcl-2 interaction (ABT199) resulted in a significant reduction in the elevated levels of S70pBcl-2 seen in M14 $Rac1^{V12}$ or CEM/Bcl-2 cells, respectively, while staurosporine treatment had only modest to no effect (Fig. 6j–k). As expected, S70E mutant expression showed much higher S70pBcl-2 expression (Fig. S11). Taken together, targeting cellular redox state and/or physical interaction between active Rac1 and S70pBcl-2 in the feedforward loop could have therapeutic implications, particularly in cancer cells exhibiting reliance on active Rac1 and/or Bcl-2.

3.6. Concordance between Rac1 and S70pBcl-2 expression in clinical lymphomas

Prompted by our findings in leukemia cell lines, we proceeded to investigate the clinical relevance of the positive loop between active Rac1 and S70pBcl-2. Firstly, analysis of lysates from primary tissue of lymphoma patients (n = 34) showed a striking positive correlation between the protein levels of Rac1 and S70pBcl-2 (Fig. 7a). Comparative statistical analyses (Pearson Correlation Coefficient; PCC) of the various permutations revealed highly significant correlations (p-values < 0.0001) between Rac1 and S70pBcl-2 (*PCC = 0.66*) and Rac1 and Bcl-2 (*PCC = 0.87*) (Fig. 7b, S12, S14). Importantly, 6 of our 34 lymphoma samples with sufficient lysates were subjected to co-IP-Western analysis for verifying the interaction between Rac1 and Bcl-2. Indeed, Rac1 co-precipitated with Bcl-2 in lysates from 4 of the 6 clinical samples (Fig. 7c). More importantly, Rac1/Bcl-2 interaction showed a strong positive correlation with S70pBcl-2 (*PCC = 0.95; p-value = 0.0038*) (Fig. 7d), and as expected with Bcl-2 (*PCC = 0.95; p-value = 0.004*) and Rac1 (*PCC = 0.94; p-value = 0.005*) (Fig. S13a-b, S14-S15).

3.7. Increased levels of Rac1 and S70pBcl-2 are associated with advanced stage lymphomas

Based on the expression analyses of Rac1, Bcl-2 and S70pBcl-2 in 34 patient lymphoma samples, we proceeded to explore the crosstalk between the two proteins in relation to disease stage/severity. Of note,

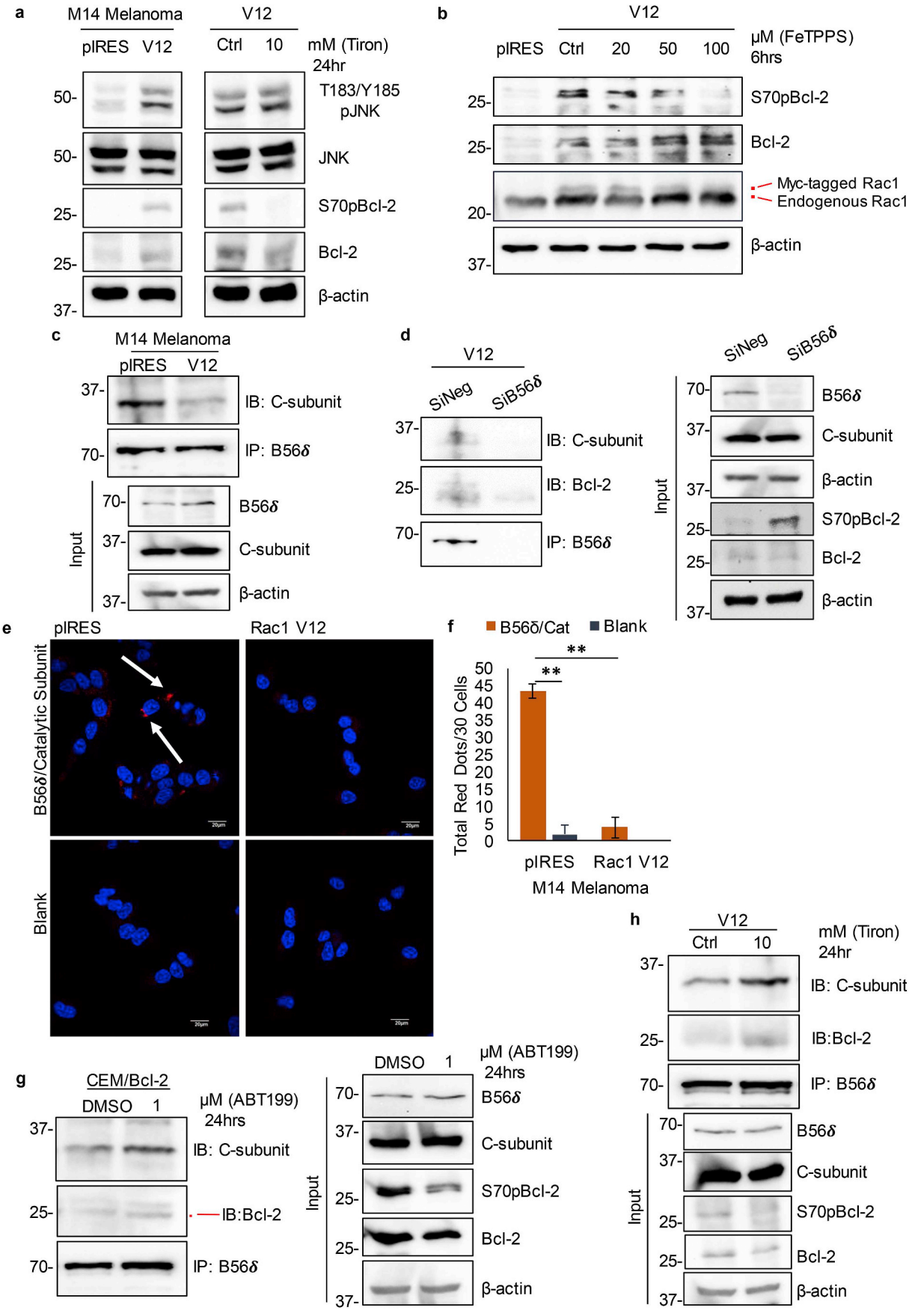

(caption on next page)

Fig. 4. Active Rac1-induced Rac1/Bcl-2 interaction is required for the inhibition of PP2A assembly in a ROS-dependent manner.
(a) Western blot analysis showing T183/Y185pJNK, JNK, S70pBcl-2, Bcl-2 and β-actin of M14 Melanoma cells stably expressing the Myc-tagged constitutively active Rac1 mutant, V12, or empty vector, pIRES as well as following 24-h treatment of 10 mM Tiron in M14 Melanoma cells stably expressing the Myc-tagged constitutively active Rac1 mutant, V12. n = 3. (b) Western blot analysis showing S70pBcl-2, Bcl-2, Rac1 and β-actin following 6-h treatment of increasing doses of FeTPPS in M14 Melanoma cells stably expressing the Myc-tagged constitutively active Rac1 mutant, V12. n = 3. (c) Western blot analysis showing the immunoprecipitation of B56δ subunit of PP2A and immunoblotting of catalytic subunit of PP2A and their respective immunoblotted inputs of B56δ, catalytic subunit and β-actin in M14 Melanoma cells stably expressing the Myc-tagged constitutively active Rac1 mutant, V12, or empty vector, pIRES. n = 3. (d) Western blot analysis showing the immunoprecipitation of B56δ subunit of PP2A and immunoblotting of catalytic subunit of PP2A and Bcl-2 and their respective immunoblotted inputs of B56δ, catalytic subunit, β-actin, S70pBcl-2, Bcl-2 and β-actin following 48-h B56δ subunit knockdown (150 nM) in M14 Melanoma cells stably expressing the Myc-tagged constitutively active Rac1 mutant, V12. n = 3. (e) PLA showing red dot appearances (white arrow) upon interaction between B56δ and catalytic subunits of PP2A in pIRES and Rac1 V12 M14 Melanoma cells. Red dots were calculated from 30 cells from randomly selected images. Blank images indicate only secondary antibodies used to check for non-specific signal. n = 3. (f) Quantification of total red dots from 30 cells from randomly selected images for target and blank samples of 3 independent sets. Bar chart displaying mean and SD. One way-ANOVA and Tukey's multiple comparisons tests were used. ** indicates P-value < 0.02. Quantitated blank values in Fig. 4f is similar to that of Fig. 2c-d as both Rac1/Bcl-2 and B56δ/Catalytic of pIRES and Rac1 V12 M14 Melanoma samples were stained and concurrently compared to the similar secondary antibody blanks. (g) Western blot analysis showing the immunoprecipitation of B56δ subunit of PP2A and immunoblotting of catalytic subunit of PP2A and Bcl-2 and their respective immunoblotted inputs of B56δ, catalytic subunit, S70pBcl-2, Bcl-2 and β-actin following 24-h treatment of 1 μM ABT199 in CEM/Bcl-2 cells. n = 3. (h) Western blot analysis showing the immunoprecipitation of B56δ subunit of PP2A and immunoblotting of catalytic subunit of PP2A and Bcl-2 and their respective immunoblotted inputs of B56δ, catalytic subunit, S70pBcl-2, Bcl-2 and β-actin following 24-h treatment of 10 mM Tiron in M14 Melanoma cells stably expressing the Myc-tagged constitutively active Rac1 mutant, V12. n = 3. (For interpretation of the references to color in this figure legend, the reader is referred to the Web version of this article.)

increased protein levels of Rac1 and S70pBcl-2 (and Bcl-2) strongly correlated with advanced stage of the disease (stage 3–4) in clinical lymphomas (Fig. 7e–g, S14); protein levels were significantly higher compared to lysates from stage 0–2 lymphomas (*S70pBcl-2: p-value = 0.011*; *Bcl-2: p-value = 0.024; Rac1: p-value = 0.037*). A similar positive correlation was observed between disease severity and Rac1/Bcl-2 interaction (Fig. 7h, S14-S15); however, statistical significance could not be determined due to the small sample size (n = 6). Furthermore, Rac1 relative mRNA level positively correlates with advanced disease stage in malignant melanoma from TCGA database (Fig. S16). Collectively, our findings strongly support the *in vivo* existence of a positive feedforward loop between active Rac1 and S70pBcl-2 in an interactive and redox-dependent manner to sustain S70pBcl-2 for cancer cell survival and progression (Fig. 8).

4. Discussion

4.1. A feedforward loop involving Active Rac1, S70pBcl-2 and their interaction is critical for S70pBcl-2 maintenance and its anti-apoptotic function

Our previous work has implicated the 'pro-oxidant' activity of active Rac1 or Bcl-2 in promoting cancer cell survival and/or chemo-resistance [5,8,9,16]. Interestingly, inhibiting Rac1 activity alleviated Bcl-2-induced increase in mitochondrial $O_2^{\cdot-}$ [8,9], thus suggesting a clear role for active Rac1 in the apoptosis inhibitory function of Bcl-2. In this report we provide evidence that GTP-loaded Rac1 (active) exhibits higher affinity for Bcl-2 and that this physical proximity promotes the sustained S70pBcl-2, which stabilizes its anti-apoptotic activity.

Intriguingly, the observation that S70pBcl-2 further enhances the binding between Bcl-2 and active Rac1 argues in favor of a positive feedforward loop to sustain S70pBcl-2. The feedforward loop between Rac1 and S70pBcl-2 is corroborated by the inability of S70A to bind to Rac1, while S70E elicited avid interaction. A plausible explanation could be that the initial binding of active Rac1 to Bcl-2 is rapid and transient, which allows for the induction of ROS-dependent S70pBcl-2 to further stabilize the binding of Rac1 to Bcl-2. Alternatively, the binding of Rac1 to Bcl-2 could happen due to JNK-mediated endogenous S70pBcl-2, thereby first prompting the binding of active Rac1 to Bcl-2 and subsequently further enhancing S70pBcl-2 through active Rac1-induced ROS.

The critical involvement of the BH3 domain and its juxtaposed non-structured loop region (contains the S70 residue) of Bcl-2 in the interaction with active Rac1 are highlighted. The use of BH3-mimetic inhibitors to disrupt Rac1/Bcl-2 interaction hints the possibility of a competitive binding between BH3-mimetic inhibitors and Rac1 at the BH3 domain of Bcl-2. Alternatively, the binding between BH3-mimetic inhibitors and Bcl-2 could change the conformation of Bcl-2, thereby disrupting the interaction between Rac1 and Bcl-2 at other domains; potentially the juxtaposed non-structured loop region. Nevertheless, our data provide support to the latter hypothesis, whereby a drop in S70pBcl-2 is accompanied by both decreases in Rac1 or NOXA interaction with Bcl-2. Reciprocally, Bcl-2 concurrently binds to both Rac1 and NOXA upon active Rac1-induced S70pBcl-2 in $Rac1^{V12}$ cells. Furthermore, Deng et al. demonstrated that maximal association of Bcl-2 to Bax requires S70pbcl-2 [26], which is correspondingly important

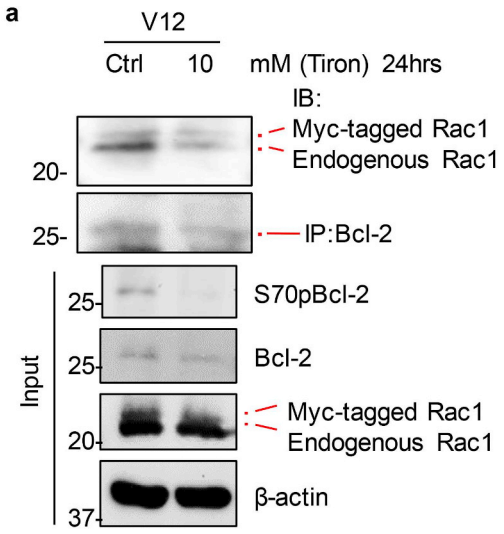

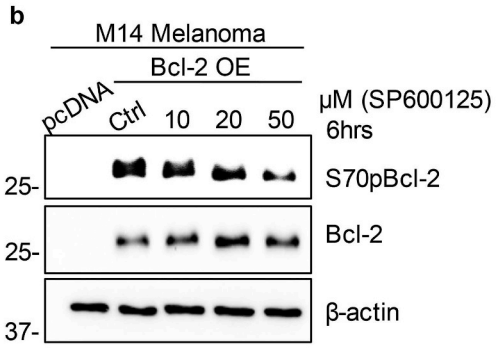

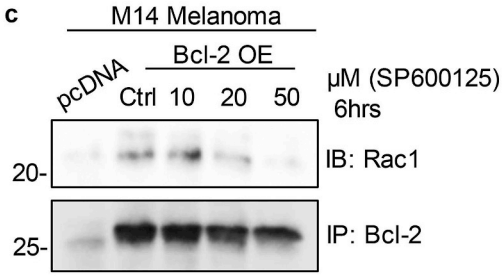

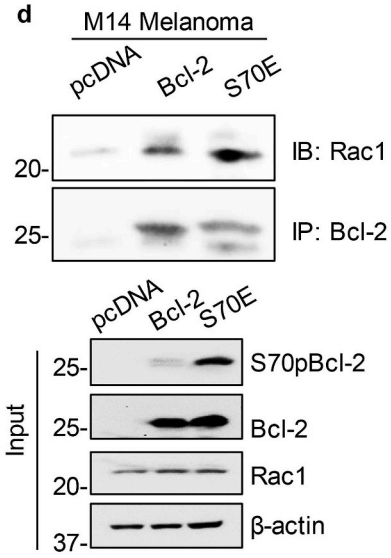

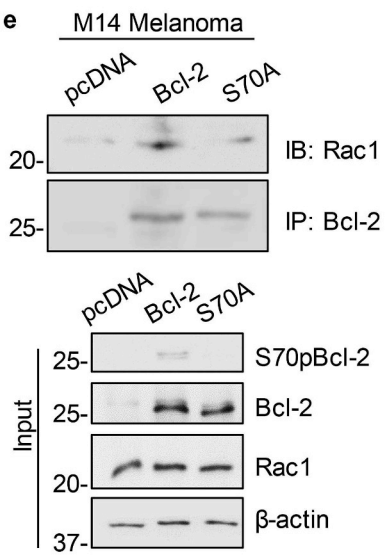

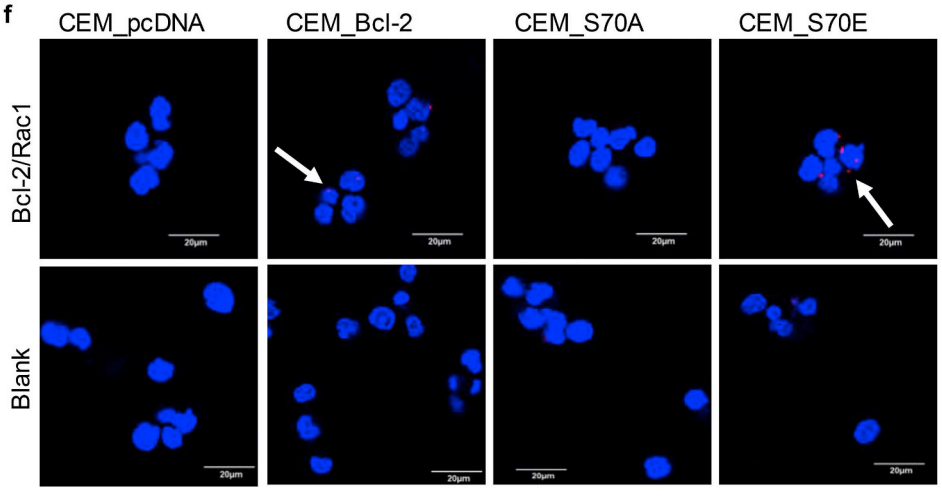

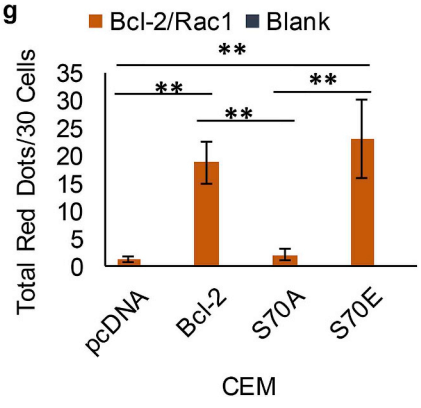

(caption on next page)

Fig. 5. S70 phosphorylation of Bcl-2 further secures interaction between Rac1 and Bcl-2.
(a) Western blot analysis showing the immunoprecipitation of Bcl-2 and immunoblotting of Rac1 following 24-h treatment of 10 mM Tiron in M14 Melanoma cells stably expressing the Myc-tagged constitutively active Rac1 mutant, V12. n = 3. (b) Western blot analysis showing S70pBcl-2, Bcl-2 and β-actin following 6-h treatment of increasing doses of JNK inhibitor, SP600125, in M14 Melanoma cells transiently transfected with wild type Bcl-2. OE: Overexpression. n = 3. (c) Western blot analysis showing the immunoprecipitation of Bcl-2 and immunoblotting of Rac1 following 6-h treatment of increasing doses of JNK inhibitor, SP600125, in M14 Melanoma cells transiently transfected with wild type Bcl-2. n = 3. (d–e) Western blot analysis showing the immunoprecipitation of Bcl-2 and immunoblotting of Rac1 in M14 Melanoma cells transiently transfected with 2 μg empty vector, pcDNA3.1, wild type (WT) Bcl-2, phosphomimetic S70E mutant Bcl-2 and non-phosphorylatable S70A mutant Bcl-2 for 48 h and their respective immunoblotted inputs of S70pBcl-2, Bcl-2, Rac1 and β-actin. n = 3. (f) PLA showing red dot appearances (white arrow) upon Bcl-2 and Rac1 interaction of CEM cells transiently transfected with 2 μg pcDNA3.1, WT Bcl-2, S70A or S70E plasmids for 48 h. Red dots were calculated from 30 cells from randomly selected images. Blank images indicate only secondary antibodies used to check for non-specific signal. n = 3. (g) Quantification of total red dots from 30 cells from randomly selected images for target and blank samples of 3 independent sets. All bar chart displaying mean and SD. One way-ANOVA and Tukey's multiple comparisons tests were used. ** indicates P-value < 0.02. (For interpretation of the references to color in this figure legend, the reader is referred to the Web version of this article.)

for Bcl-2/Rac1 binding. On the other hand, as Rac1 status is implicated in the interaction between Rac1 and Bcl-2, interests arise if other gain-of-function Rac1 mutations, such as $Rac1^{P29S}$ and Rac1b [6,27–30], could also contribute to the interaction between Rac1 and Bcl-2 via a potential change in Rac1 conformation, its activation status or affinity towards Bcl-2. With that said, narrowing down the actual interacting domains of Bcl-2 and Rac1 would undoubtedly provide important information in the specific targeting of Rac1/Bcl-2 interaction and the resultant S70pBcl-2.

Notably, our data also demonstrated that $Rac1^{V12}$ could stabilize Bcl-2 protein. Indeed, $Rac1^{V12}$ could induce an increase in T69pBcl-2, which has been shown to stabilize Bcl-2 protein via Pyruvate Kinase M2 (PKM2) [31]. Nevertheless, our data showed that T69pBcl-2 is not regulated by $O_2^{\cdot-}$, suggesting that while T69pBcl-2 could stabilize Bcl-2, it does not take part in the redox regulation of Bcl-2/Rac1 interaction and S70pBcl-2 induction. Nonetheless, as JNK and PKM2 could phosphorylate Bcl-2 [25,31], it is possible that T69pBcl-2 is a function of active Rac1-induced JNK or PKM2 activation [32].

4.2. Active Rac1-induced S70pBcl-2 involves the interaction of Rac1 with Bcl-2 as well as its redox activity to inhibit PP2A assembly

While S70pBcl-2 is phosphorylated by JNK [25], we demonstrated that Rac1-induced S70pBcl-2 via $O_2^{\cdot-}$ is not JNK-dependent but more relevantly the redox-dependent inhibition of PP2A holoenzyme assembly. To that end, PP2A functions as a putative tumor suppressor by regulating the phosphorylation-dependent activation/stability of oncogenic proteins such as c-Myc, Akt, IKK and Bcl-2 [5,33–35]. Moreover, PP2A has been shown to bind to and regulate Rac1 activity, thus influencing Rac1-mediated migration/invasion [36]. Intrigued by the involvement of active Rac1 in not only creating a 'pro-oxidant' milieu but also in promoting sustained S70pBcl-2, we questioned whether the latter was a function of disrupting PP2A-mediated dephosphorylation of S70pBcl-2. Our present work indeed re-capitulated the redox-dependent inhibition of PP2A-B56δ assembly [5], resulting in an increase in S70pBcl-2 in a Rac1-dependent manner. In addition, as S70pBcl-2 binds to active Rac1 and B56δ, it is plausible that B56δ-bound S70pBcl-2 places B56δ in close proximity of active Rac1 and amenable to redox-dependent modification. This hypothesis is plausible as our previous *in vivo* work demonstrated that B56δ-bound S70pBcl-2 has disrupted interaction with PP2A C-subunit [5], which is in accordance to our present *in vivo* evidence that S70pBcl-2 is highly bound to Rac1.

4.3. Increased Rac1 and S70pBcl-2 as predictive marker(s) of advanced disease as well as potential nodes for therapeutic strategy against refractory tumors

Our findings demonstrate that active Rac1, S70pBcl-2 and their physical interaction function in tandem to promote survival and drug resistance. Of note, this functional synergy is verified in clinical samples obtained from patients with lymphoma; levels of Rac1, S70pBcl-2 (and Bcl-2) and their interaction are positively correlated with higher stage lymphomas, thereby underscoring the presence of a novel crosstalk that maintains a conducive cellular redox environment for the growth and progression of cancer cells. Based on the strong clinical correlation, one is tempted to speculate that the co-expression of Rac1 and S70pBcl-2 as well as their physical interaction could serve as markers for disease stratification and potential nodes for therapeutic intervention. The latter would highlight the potential of novel combinational approaches to target S70pBcl-2, particularly with drugs that are FDA-approved [37–41]. As a proof-of-concept, we provide evidence that combinational approach using tiron or ABT199 with staurosporine, significantly

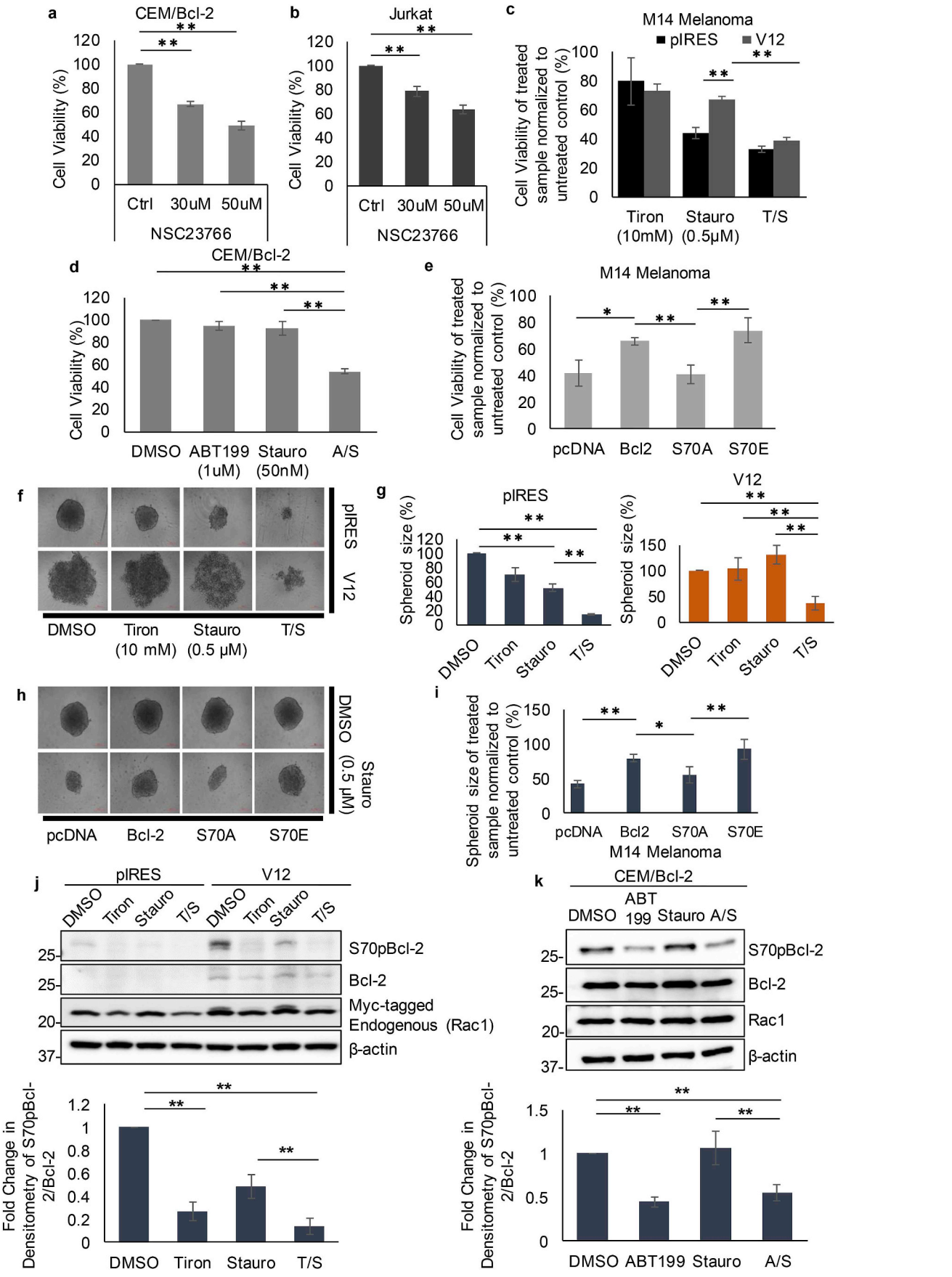

(caption on next page)

Fig. 6. Pharmacological interventions targeting the active Rac1-induced S70pBcl-2 loop sensitizes to apoptotic stimulus.
(a–b) Measurement of cell viability (%) of CEM/Bcl-2 and Jurkat cells following 24-h treatment of increasing doses of NSC23766. n = 3. (c) Measurement of cell viability of pIRES and Rac1 (V12) M14 Melanoma cells following 1-h pre-treatment of 10 mM Tiron and subsequent 24-h treatment of 0.5 μM of staurosporine. Cell viability of tiron and/or staurosporine-treated cells normalized to that of untreated cells in (%). n = 3. (d) Measurement of cell viability (%) of CEM/Bcl-2 cells following 1-h pre-treatment of 1 μM ABT199 and subsequent 24-h treatment of 50 nM of staurosporine. n = 3. (e) Measurement of cell viability of M14 Melanoma cells transiently transfected with pcDNA3.1, WT Bcl-2, S70A and S70E following 24-h treatment of 0.5 μM of staurosporine. Cell viability of staurosporine-treated cells normalized to that of untreated cells in (%). n = 3. (f) 72-h spheroid formation of pIRES and Rac1 (V12) M14 Melanoma cells following 1-h pre-treatment of 10 mM Tiron and subsequent 24-h treatment of 0.5 μM of staurosporine. n = 3. (g) Quantification of spheroid size (%) of pIRES and Rac1 (V12) M14 Melanoma cells following 1-h pre-treatment of 10 mM Tiron and subsequent 24-h treatment of 0.5 μM of staurosporine. (h) 72-h spheriod formation of M14 Melanoma cells transiently transfected with empty vector pcDNA3.1, wild-type Bcl-2, non-phosphorylatable S70A mutant Bcl-2 and phosphomimetic S70E mutant Bcl-2 following 24-h treatment of 0.5 μM of staurosporine. n = 3. (i) Quantification of spheroid size of M14 Melanoma cells transiently transfected with empty vector pcDNA3.1, wild-type Bcl-2, non-phosphorylatable S70A mutant Bcl-2 and phosphomimetic S70E mutant Bcl-2 following 24-h treatment of 0.5 μM of staurosporine. Spheroid size of staurosporine-treated cells normalized to that of untreated cells in (%). (j) Western Blot analysis showing S70pBcl-2, Bcl-2, Rac1 and β-actin following 1-h pre-treatment of 10 mM Tiron and subsequent 24-h treatment of 0.5 μM of staurosporine in pIRES and Rac1 (V12) M14 Melanoma cells. n = 4. Bar charts showing fold change in densitometry of S70pBcl-2 normalized to Bcl-2. (k) Western Blot analysis showing S70pBcl-2, Bcl-2, Rac1 and β-actin following 1-h pre-treatment of 1 μM ABT199 and subsequent 24-h treatment of 50 nM of staurosporine. n = 3. Bar charts showing fold change in densitometry of S70pBcl-2 normalized to Bcl-2. All bar chart displaying mean and SD. One way-ANOVA and Tukey's multiple comparisons tests were used. * and ** indicates P-value < 0.05 and 0.02 respectively.

amplifies drug sensitivity of cancer cells by inhibiting S70pBcl-2. Collectively, these observations indicate that targeting the feedforward loop could be an excellent chemo-sensitizer particularly in Rac1-or S70pBcl-2-driven malignancies.

Conflict of interest disclosures

The following authors have affiliations with following organizations, with direct or indirect financial interest. Shireen Vali and Taher Abbasi are affiliated with Cellworks Group, Inc., San Jose, CA, a precision medicine company using simulation modelling and Ansu Kumar works for Cellworks Research India Limited, Bangalore, India, a fully owned subsidiary of Cellworks Group Inc. The other authors express no conflicts of interest.

CRediT authorship contribution statement

Stephen Jun Fei Chong: Conceptualization, Methodology, Validation, Formal analysis, Investigation, Writing - original draft, Writing - review & editing, Visualization, Supervision, Project administration. **Jolin Xiao Hui Lai:** Methodology, Validation, Formal analysis, Investigation, Writing - original draft, Visualization. **Jianhua Qu:** Software, Validation, Formal analysis, Investigation, Visualization. **Jayshree Hirpara:** Investigation, Data curation, Writing - original draft. **Jia Kang:** Conceptualization, Methodology, Writing - original draft. **Kunchithapadam Swaminathan:** Conceptualization, Methodology, Validation, Supervision, Resources, Writing - review & editing. **Thomas Loh:** Resources, Formal analysis, Investigation. **Ansu Kumar:** Software, Formal analysis, Visualization. **Shireen Vali:** Software, Formal analysis, Visualization. **Taher Abbasi:** Software, Formal analysis, Visualization. **Shazib Pervaiz:** Conceptualization, Methodology, Validation, Writing - original draft, Writing - review & editing, Resources, Supervision, Project administration, Funding acquisition.

Acknowledgments

This work was supported by the National Medical Research Council of Singapore (NMRC/CIRG/1433/2015) and Ministry of Education Tier 2 of Singapore (MOE2013-T2-2-130). We thank Marie V. Clement (NUS) for providing us the human M14 melanoma pIRES and $Rac1^{V12}$ cell lines. We thank Roberta A. Gottlieb (Cedars-Sinai) for providing us the CEM/Neo and CEM/Bcl-2 cell lines. We thank David M. Virshup (DUKE-NUS) for providing us the Rabbit polyconal anti-B56δ (UT98) antibody. We thank Elizabeth Yang (Vanderbilt University) for providing us the pcDNA3.1 vector plasmid. We thank Askhaya Krishnagopal for providing technical support to this study.

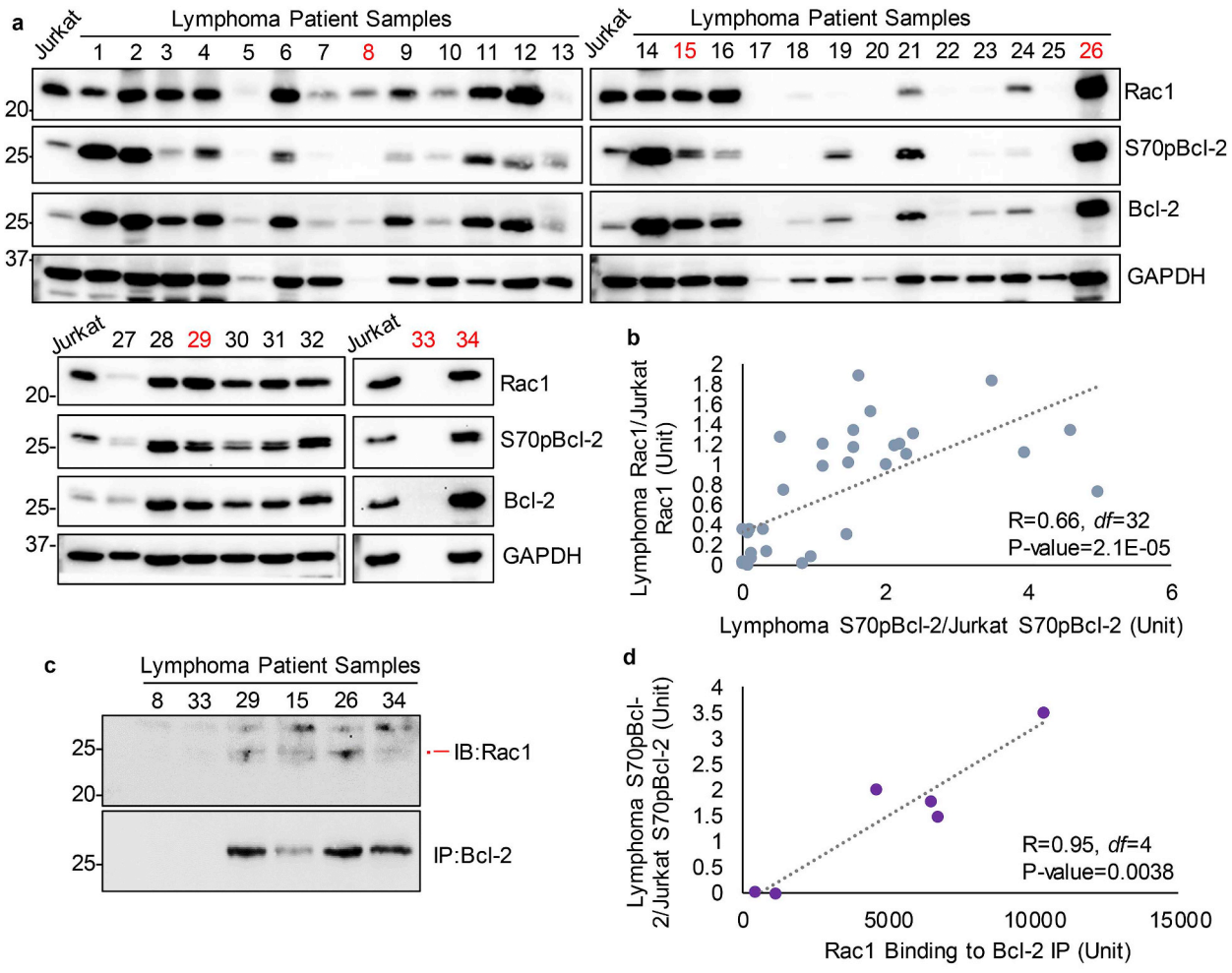

(caption on next page)

Fig. 7. Rac1 and S70pBcl-2 expression as well as S70pBcl-2 and Rac1/Bcl-2 interaction are positively correlated and implicated in more advanced stage lymphomas.

(a) Western Blot analysis showing S70pBcl-2, Bcl-2, Rac1 and GAPDH of 34 patient lymphoma samples. Jurkat cell lysate is used as a control. n = 1. A more detailed clinical diagnosis of these lymphoma samples is displayed in Supplementary Fig. S14. (b) Scatter plot showing the positive correlation of protein band densities (arbitrary unit) normalized to their respective control proteins from Jurkat lysate of Rac1 and S70pBcl-2 of 34 patient lymphoma samples as well as their respective Pearson correlation coefficient, R, and P values. P-value is calculated using ANOVA. Raw values are displayed in Supplementary Fig. S14. (c) Western blot analysis showing the immunoprecipitation of Bcl-2 and immunoblotting of Rac1 of 6 lymphoma patient samples. Input is displayed in Fig. 7a labelled in red patient numbers. n = 1. (d) Scatter plot showing the positive correlation of protein band densities (arbitrary unit) normalized to their respective control proteins from Jurkat lysate of S70pBcl-2 against density of Rac1 from immunoprecipitated Bcl-2 of 6 patient lymphoma samples as well as their respective Pearson correlation coefficient, R, and P-values. P-value is calculated using ANOVA. Raw values are displayed in Supplementary Figs. S14 and S15. (e–h) Box plots showing the correlations of S70pBcl-2, Bcl-2, Rac1 and Rac1/Bcl-2 Binding to tumor stages of lymphoma patient samples. Raw values are displayed in Supplementary Figs. S14 and S15. Box plot displaying median, inter-quartiles and whiskers in horizontal lines and mean in "x". P-value is calculated using paired T test. (For interpretation of the references to color in this figure legend, the reader is referred to the Web version of this article.)

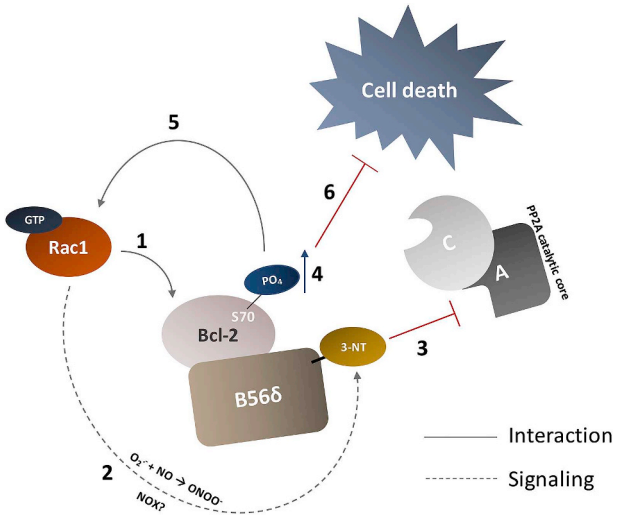

Fig. 8. Diagram depicting the crosstalk between active Rac1 and S70pBcl-2.

(1) Active Rac1 binds to Bcl-2, thereby permitting Rac1 to be in close proximity of Bcl-2-bound B56δ for (2) NOX/$O_2^{\cdot-}$- and $ONOO^-$-mediated nitration and (3) inhibition of PP2A assembly. (4) This reciprocally induces the accumulation of kinase (JNK)-induced S70pBcl-2, which in turn (5) further secures the binding between Bcl-2 and active Rac1, resulting to a positive feedforward loop. This loop potentially sustains S70pBcl-2 and thereby (6) inhibits cell death.

Appendix A. Supplementary data

Supplementary data to this article can be found online at https://doi.org/10.1016/j.canlet.2019.05.009.

References

[1] E. Panieri, M.M. Santoro, ROS homeostasis and metabolism: a dangerous liason in cancer cells, Cell Death Dis. 7 (2016) e2253.

[2] F. Weinberg, R. Hamanaka, W.W. Wheaton, S. Weinberg, J. Joseph, M. Lopez, B. Kalyanaraman, G.M. Mutlu, G.R. Budinger, N.S. Chandel, Mitochondrial metabolism and ROS generation are essential for Kras-mediated tumorigenicity, Proc. Natl. Acad. Sci. U. S. A. 107 (2010) 8788–8793.

[3] D. Hanahan, R.A. Weinberg, The hallmarks of cancer, Cell 100 (2000) 57–70.

[4] P.S. Hole, J. Zabkiewicz, C. Munje, Z. Newton, L. Pearn, P. White, N. Marquez, R.K. Hills, A.K. Burnett, A. Tonks, R.L. Darley, Overproduction of NOX-derived ROS in AML promotes proliferation and is associated with defective oxidative stress signaling, Blood 122 (2013) 3322–3330.

[5] I.C. Low, T. Loh, Y. Huang, D.M. Virshup, S. Pervaiz, Ser70 phosphorylation of Bcl-2 by selective tyrosine nitration of PP2A-B56delta stabilizes its antiapoptotic activity, Blood 124 (2014) 2223–2234.

[6] S.J.F. Chong, J.X.H. Lai, J.Q. Eu, G.L. Bellot, S. Pervaiz, Reactive oxygen species and oncoprotein signaling-A dangerous liaison, Antioxidants Redox Signal. 29 (2018) 1553–1588.

[7] G.Y. Liou, H. Doppler, K.E. DelGiorno, L. Zhang, M. Leitges, H.C. Crawford, M.P. Murphy, P. Storz, Mutant KRas-induced mitochondrial oxidative stress in acinar cells upregulates EGFR signaling to drive formation of pancreatic precancerous lesions, Cell Rep. 14 (2016) 2325–2336.

[8] S. Pervaiz, J. Cao, O.S. Chao, Y.Y. Chin, M.V. Clement, Activation of the RacGTPase inhibits apoptosis in human tumor cells, Oncogene 20 (2001) 6263–6268.

[9] R. Velaithan, J. Kang, J.L. Hirpara, T. Loh, B.C. Goh, M. Le Bras, C. Brenner, M.V. Clement, S. Pervaiz, The small GTPase Rac1 is a novel binding partner of Bcl-2 and stabilizes its antiapoptotic activity, Blood 117 (2011) 6214–6226.

[10] B. Debreceni, Y. Gao, F. Guo, K. Zhu, B. Jia, Y. Zheng, Mechanisms of guanine nucleotide exchange and Rac-mediated signaling revealed by a dominant negative trio mutant, J. Biol. Chem. 279 (2004) 3777–3786.

[11] J. Wang, Q. Rao, M. Wang, H. Wei, H. Xing, H. Liu, Y. Wang, K. Tang, L. Peng, Z. Tian, J. Wang, Overexpression of Rac1 in leukemia patients and its role in leukemia cell migration and growth, Biochem. Biophys. Res. Commun. 386 (2009) 769–774.

[12] T. Tian, C. Bi, A.L. Hein, X. Zhang, C. Wang, S. Shen, J. Yuan, T.C. Greiner, C. Enke, J. Vose, Y. Yan, K. Fu, Rac1 is a novel therapeutic target in mantle cell lymphoma, Blood Canc. J. 8 (2018) 17.

[13] A.L. Hein, C.M. Post, Y.M. Sheinin, I. Lakshmanan, A. Natarajan, C.A. Enke, S.K. Batra, M.M. Ouellette, Y. Yan, RAC1 GTPase promotes the survival of breast cancer cells in response to hyper-fractionated radiation treatment, Oncogene 35 (2016) 6319–6329.

[14] Z.X. Chen, S. Pervaiz, Bcl-2 induces pro-oxidant state by engaging mitochondrial respiration in tumor cells, Cell Death Differ. 14 (2007) 1617–1627.

[15] Z.X. Chen, S. Pervaiz, Involvement of cytochrome c oxidase subunits Va and Vb in the regulation of cancer cell metabolism by Bcl-2, Cell Death Differ. 17 (2010) 408–420.

[16] M.V. Clement, J.L. Hirpara, S. Pervaiz, Decrease in intracellular superoxide sensitizes Bcl-2-overexpressing tumor cells to receptor and drug-induced apoptosis independent of the mitochondria, Cell Death Differ. 10 (2003) 1273–1285.

[17] X. Deng, F. Gao, T. Flagg, J. Anderson, W.S. May, Bcl2's flexible loop domain regulates p53 binding and survival, Mol. Cell. Biol. 26 (2006) 4421–4434.

[18] X. Deng, F. Gao, T. Flagg, W.S. May Jr., Mono- and multisite phosphorylation enhances Bcl2's antiapoptotic function and inhibition of cell cycle entry functions, Proc. Natl. Acad. Sci. U. S. A. 101 (2004) 153–158.

[19] X. Deng, F. Gao, W.S. May Jr., Bcl2 retards G1/S cell cycle transition by regulating intracellular ROS, Blood 102 (2003) 3179–3185.

[20] X. Deng, P. Ruvolo, B. Carr, W.S. May Jr., Survival function of ERK1/2 as IL-3-activated, staurosporine-resistant Bcl2 kinases, Proc. Natl. Acad. Sci. U. S. A. 97 (2000) 1578–1583.

[21] T. Ito, X. Deng, B. Carr, W.S. May, Bcl-2 phosphorylation required for anti-apoptosis function, J. Biol. Chem. 272 (1997) 11671–11673.

[22] X. Deng, F. Gao, W.S. May, Protein phosphatase 2A inactivates Bcl2's antiapoptotic function by dephosphorylation and up-regulation of Bcl2-p53 binding, Blood 113 (2009) 422–428.

[23] Y. Wei, S. Pattingre, S. Sinha, M. Bassik, B. Levine, JNK1-mediated phosphorylation of Bcl-2 regulates starvation-induced autophagy, Mol. Cell 30 (2008) 678–688.

[24] S. Pattingre, C. Bauvy, S. Carpentier, T. Levade, B. Levine, P. Codogno, Role of JNK1-dependent Bcl-2 phosphorylation in ceramide-induced macroautophagy, J. Biol. Chem. 284 (2009) 2719–2728.

[25] K. Maundrell, B. Antonsson, E. Magnenat, M. Camps, M. Muda, C. Chabert, C. Gillieron, U. Boschert, E. Vial-Knecht, J.C. Martinou, S. Arkinstall, Bcl-2 undergoes phosphorylation by c-Jun N-terminal kinase/stress-activated protein kinases in the presence of the constitutively active GTP-binding protein Rac1, J. Biol. Chem. 272 (1997) 25238–25242.

[26] X. Deng, S.M. Kornblau, P.P. Ruvolo, W.S. May Jr., Regulation of Bcl2 phosphorylation and potential significance for leukemic cell chemoresistance, J. Natl. Cancer Inst. Monogr. (2001) 30–37.

[27] M.J. Davis, B.H. Ha, E.C. Holman, R. Halaban, J. Schlessinger, T.J. Boggon, RAC1P29S is a spontaneously activating cancer-associated GTPase, Proc. Natl. Acad. Sci. U. S. A. 110 (2013) 912–917.

[28] D.C. Radisky, D.D. Levy, L.E. Littlepage, H. Liu, C.M. Nelson, J.E. Fata, D. Leake, E.L. Godden, D.G. Albertson, M.A. Nieto, Z. Werb, M.J. Bissell, Rac1b and reactive oxygen species mediate MMP-3-induced EMT and genomic instability, Nature 436 (2005) 123–127.

[29] C. Melzer, R. Hass, J. von der Ohe, H. Lehnert, H. Ungefroren, The role of TGF-beta and its crosstalk with RAC1/RAC1b signaling in breast and pancreas carcinoma, Cell Commun. Signal. : CCS 15 (2017) 19.

[30] T. Tomino, H. Tajiri, T. Tatsuguchi, T. Shirai, K. Oisaki, S. Matsunaga, F. Sanematsu, D. Sakata, T. Yoshizumi, Y. Maehara, M. Kanai, J.F. Cote, Y. Fukui, T. Uruno, DOCK1 inhibition suppresses cancer cell invasion and macropinocytosis induced by self-activating Rac1(P29S) mutation, Biochem. Biophys. Res. Commun. 497 (2018) 298–304.

[31] J. Liang, R. Cao, X. Wang, Y. Zhang, P. Wang, H. Gao, C. Li, F. Yang, R. Zeng, P. Wei, D. Li, W. Li, W. Yang, Mitochondrial PKM2 regulates oxidative stress-induced apoptosis by stabilizing Bcl2, Cell Res. 27 (2017) 329–351.
[32] A. Gupta, A. Ajith, S. Singh, R.K. Panday, A. Samaiya, S. Shukla, PAK2-c-Myc-PKM2 axis plays an essential role in head and neck oncogenesis via regulating Warburg effect, Cell Death Dis. 9 (2018) 825.
[33] R. Breuer, M.S. Becker, M. Brechmann, T. Mock, R. Arnold, P.H. Krammer, The protein phosphatase 2A regulatory subunit B56gamma mediates suppression of T cell receptor (TCR)-induced nuclear factor-kappaB (NF-kappaB) activity, J. Biol. Chem. 289 (2014) 14996–15004.
[34] Y.C. Kuo, K.Y. Huang, C.H. Yang, Y.S. Yang, W.Y. Lee, C.W. Chiang, Regulation of phosphorylation of Thr-308 of Akt, cell proliferation, and survival by the B55alpha regulatory subunit targeting of the protein phosphatase 2A holoenzyme to Akt, J. Biol. Chem. 283 (2008) 1882–1892.
[35] C.M. Lucas, R.J. Harris, A. Giannoudis, M. Copland, J.R. Slupsky, R.E. Clark, Cancerous inhibitor of PP2A (CIP2A) at diagnosis of chronic myeloid leukemia is a critical determinant of disease progression, Blood 117 (2011) 6660–6668.
[36] J.P. ten Klooster, I. Leeuwen, N. Scheres, E.C. Anthony, P.L. Hordijk, Rac1-induced cell migration requires membrane recruitment of the nuclear oncogene SET, EMBO J. 26 (2007) 336–345.
[37] M.S. Davids, A. Letai, ABT-199: taking dead aim at BCL-2, Cancer Cell 23 (2013) 139–141.
[38] E.D. Deeks, Venetoclax: first global approval, Drugs 76 (2016) 979–987.
[39] M.S. Davids, Targeting BCL-2 in B-cell lymphomas, Blood 130 (2017) 1081–1088.
[40] C.S. Tam, M.A. Anderson, C. Pott, R. Agarwal, S. Handunnetti, R.J. Hicks, K. Burbury, G. Turner, J. Di Iulio, M. Bressel, D. Westerman, S. Lade, M. Dreyling, S.J. Dawson, M.A. Dawson, J.F. Seymour, A.W. Roberts, Ibrutinib plus venetoclax for the treatment of mantle-cell lymphoma, N. Engl. J. Med. 378 (2018) 1211–1223.
[41] J.F. Seymour, T.J. Kipps, B. Eichhorst, P. Hillmen, J. D'Rozario, S. Assouline, C. Owen, J. Gerecitano, T. Robak, J. De la Serna, U. Jaeger, G. Cartron, M. Montillo, R. Humerickhouse, E.A. Punnoose, Y. Li, M. Boyer, K. Humphrey, M. Mobasher, A.P. Kater, Venetoclax-rituximab in relapsed or refractory chronic lymphocytic leukemia, N. Engl. J. Med. 378 (2018) 1107–1120.